ESO-Based Controller With Model Predictive Governor for 3D Trajectory Tracking of Underactuated Underwater Vehicles

Shihan Kong, Jinlin Sun, Changlin Qiu, Zhengxing Wu, and Junzhi Yu, *Senior Member, IEEE*

***Abstract*—In this paper, an extended state observer (ESO)-based controller with a model predictive governor is designed for 3D trajectory tracking of underactuated underwater vehicles. The proposed control scheme takes three primary challenges including underactuated property, velocity constraint, and lumped disturbance into consideration. With respect to the model predictive governor, an underactuated kinematic tracking error model is utilized to produce reference velocities. Meanwhile, a heading angle compensation mechanism is utilized to avoid the steady tracking errors resulting from dynamics coupling of the vehicle. Besides, an ESO is designed to estimate the lumped disturbances and unmeasured velocity states. Based on the ESO, a kinetic controller is offered to accomplish the precise velocity tracking only in virtue of the position and orientation information. Note that this paper details both the design process of the control scheme and rigorous theoretical analysis. Eventually, simulation and experimental results demonstrate the feasibility and superiority of the proposed method. Notably, this work lays the foundation for the underactuated trajectory tracking control in complicated and turbulent underwater environments.**

***Index Terms*—Underactuated underwater vehicle, model predictive control, robust control, 3D trajectory tracking, extended state observer.**

I. Introduction

In recent years, there are numerous applications of underwater vehicles in marine and industry fields [1]–[4]. The primary technological challenges of underwater vehicles are three-fold, i.e., underactuation, velocity constraints, and lumped disturbances including parameters uncertainties and external disturbances [5]–[8]. To guarantee the precise underwater operation, it is necessary to design the high-quality motion controller to tackle the aforementioned problems [9]–[11]. Especially, the 3D trajectory tracking control, which is aimed to follow a referenced path associated with a timing law for reaching certain positions, is a more complicated task among the motion control fields [12].

Underactuated mechanism is widely employed in underwater vehicles, for it can greatly simplify the mechanical structure of vehicles. However, the underactuated property leads to a much more difficult control task due to the overpossession of degrees of freedom (DOF) beyond the control inputs [6], i.e., the number of actuators is less than the vehicle's motion DOF [12]. To exploit the trajectory tracking control of underactuated underwater vehicles, there are numerous conventional methodologies in the literature, which include PID controller [13], neural network controller [14], fuzzy controller [15], sliding mode controller [16], adaptive controller [12], and backstepping controller [4]. Summarized from the aforementioned technologies, there is a classical control scheme for general underactuated underwater vehicles, which consists of a velocity reference governor producing expectational velocities and a robust element tackling disturbances and parameter uncertainties.

Generally, the reference governor can generate expectational velocities to ensure the underwater vehicle efficiently tracking the reference trajectory kinematically. As is indicated in [4], [12], [15], the reference governor is regarded as a kinematical controller designed by the Lyapunov-based principles, which neglects the velocity constraints. Inspired by [17]–[19], the optimization-based reference governors are appropriate to ensure that the constraints are satisfied. In recent years, the model predictive control (MPC) method, as a crucial branch of the optimal control [20], has been diffusely implemented for the nonlinear multiple-input and multiple-output systems with constraints [21], [22]. Various MPC-based control methodologies have been proposed for underwater vehicles in the literature [23]–[26]. Representatively, Rath *et al.* combined extreme learning with NMPC to accomplish the path following control [24]. Shen *et al.* introduced a Lyapunov formation constraint to the classical NMPC method to improve the robustness of the underwater vehicle control system [25]. Heshmati-Alamdari *et al.* provided a robust MPC method considering the ocean current velocities and obstacles constraints [26]. The similar characteristic of the aforementioned typical methods is that the NMPC scheme is exploited to accomplish an end-to-end feedback control by converting the dynamic model, the kinematical model, and other environmental limitations to the nonlinear constraints. Note that the NMPC simplifies the whole control process

This work was supported in part by the National Natural Science Foundation of China under Grant U1909206, Grant 61725305, Grant 61633004, Grant 61633020, and Grant 62073196. *(Corresponding author: Junzhi Yu.)*

S. Kong, C. Qiu, and Z. Wu are with the State Key Laboratory of Management and Control for Complex Systems, Institute of Automation, Chinese Academy of Sciences, Beijing 100190, China, and also with the School of Artificial Intelligence, University of Chinese Academy of Sciences, Beijing 100049, China (e-mail: kongshihan2016@ia.ac.cn; qiuchanglin2019@ia.ac.cn; zhengxing.wu@ia.ac.cn).

J. Sun is with the Institut of Automation, Chinese Academy of Sciences, Beijing 100190, China, and also with the School of Artificial Intelligence, University of Chinese Academy of Sciences, Beijing 100049, China (e-mail: jinlinsun@outlook.com).

J. Yu is with the State Key Laboratory of Management and Control for Complex Systems, Institute of Automation, Chinese Academy of Sciences, Beijing 100190, China, and also with the State Key Laboratory for Turbulence and Complex Systems, Department of Advanced Manufacturing and Robotics, BIC-ESAT, College of Engineering, Peking University, Beijing 100871, China (e-mail: junzhi.yu@ia.ac.cn).

but increases the computational burden. In practice, the linear MPC, which can be solved by the quadratic programming (QP) efficiently, is more appropriate to the online optimization-based governor [22].

The robust element of the control scheme is in charge of suppressing unknown disturbances and model perturbations. A mainstream efficient tool is to design an observer to estimate the unknown and unmeasured disturbances. The classical observer-based control methods range from sliding model observer [27], high-gain observer [28], to extended state observer (ESO) [29]. Noticeably, ESO is an essential part of the active disturbance rejection control (ADRC) framework. By using ESO, not only the lumped uncertainty including external disturbances and model parameter perturbation can be estimated, but also the velocity states can be obtained. Therefore, the control scheme is capable to accomplish the disturbance rejection trajectory tracking control only by utilizing the position and orientation information. Nowadays, Cui *et al.* proposed a novel adaptive ESO and combined it with the sliding mode controller for a full-actuated underwater vehicle trajectory tracking task [11]. Peng *et al.* utilized ESO to accomplish path following control for an underactuated underwater vehicle on the vertical plane [17]. However, there is few work about utilizing ESO equipped with optimization-based governor to the underactuated 3D trajectory tracking control to our best knowledge.

The primary contributions of this paper are summarized into three parts.

1) To tackle the general technical challenges, i.e., underactuated property, velocity constraint, and lumped disturbance, an ESO-based control scheme with model predictive governor is provided for precise 3D trajectory tracking.
2) A linear kinematical MPC is implemented on underactuated 3D trajectory tracking error model to generate reference velocities with constraints about upper and lower bound, velocity jump range, and velocity smoothness. Additionally, a heading angle compensation mechanism acts an important role for eliminating the steady state error.
3) ESO is designed to estimate the velocity states and lumped disturbance, which only requires position and orientation information. Rigorous proofs of ESO and ESO-based controller are given. Furthermore, the comparison between the method in [12] and conventional PID in the simulation demonstrates the superior performance of this controller. The laboratorial experimental verification offers insight into the underactuated trajectory tracking control in complicated and turbulent underwater environments.

The rest of the paper is organized as follows. The dynamics model and problem formulation are described in Section II. Next, the model predictive governor is designed in Section III. Then, Section IV includes the design of ESO-based controller and is followed by simulation analysis and experimental verification in Section V. Finally, the conclusion and future work are summarized in Section VI.

II. Problem Formulation

A. Underwater Vehicle Modeling

The modeling object in this manuscript is an underwater vehicle which can be actuated by the force in surge, the toque in yaw, and the force in heave, as well as it has the decoupling vertical movement relative to the horizontal movement. Thereinto, the horizontal movement is underactuated. Due to the 3D trajectory including movements on the horizontal plane and the vertical plane, the trajectory tracking movement can be considered underactuated overall. To simplify the control law design, angular velocities $[p,q]^T$ and orientations $[\phi,\theta]^T$ can be neglected. Referring to the typical underwater modeling methods in [30], the 4-DOFs motion of the underactuated underwater vehicle can be modeled kinematically by

$$\dot{\eta} = \mathbf{J}(\eta)\mu \tag{1}$$

and in kinetics by

$$\mathbf{M}\dot{\mu} + \mathbf{C}(\mu)\mu + \mathbf{D}(\mu)\mu + \mathbf{g}(\eta) = \tau_E + \tau \tag{2}$$

where $\eta = [x, y, z, \psi]^T$ is the position and orientation vector, $\mu = [u, v, w, r]^T$ is the velocity vector, $\tau = [\tau_u, 0, \tau_w, \tau_r]^T$ is the underactuated actuator vector, $\tau_E = [\tau_{du}, \tau_{dv}, \tau_{dw}, \tau_{dr}]^T$ presents the vector of external disturbances, $\mathbf{M}$ is the body mass matrix, $\mathbf{C}(\mu)$ denotes the Coriolis and centripetal matrix, $\mathbf{D}(\mu)$ is the drag matrix, and $\mathbf{g}(\eta)$ signifies the hydrostatic force vector. Besides, $\mathbf{J}(\eta)$ represents the transformation matrix with the description as follows:

$$\mathbf{J}(\eta) = \begin{bmatrix} \cos(\psi) & -\sin(\psi) & 0 & 0 \\ \sin(\psi) & \cos(\psi) & 0 & 0 \\ 0 & 0 & 1 & 0 \\ 0 & 0 & 0 & 1 \end{bmatrix}. \tag{3}$$

In practice, it is difficult to obtain the accurate hydrodynamics coefficients of $\mathbf{M}$, $\mathbf{C}(\mu)$, $\mathbf{D}(\mu)$, and $\mathbf{g}(\eta)$ in the kinetic model (2). These four coefficients can be divided into two parts, i.e., the nominal value part and the uncertain value part which denotes the error between the true value and the nominal value. Thereinto, the nominal value part can be obtained by computational fluid dynamics (CFD) or the tower tank experiment analysis [3]. However, the nominal value of the body mass matrix is more reliable among the four coefficients. Therefore, it will simplify the model expression by modeling only with the explicit expression of $\mathbf{M}$.

With the explicit expression of $\mathbf{M}$ and the implicit expression of the other three hydrodynamics coefficients, the kinetic model of underwater vehicles can be rewritten as

$$\mathbf{M}\dot{\mu} = \mathbf{U}(\eta, \mu) + \tau_E + \tau \tag{4}$$

where $\mathbf{U}(\eta,\mu) = -\mathbf{C}(\mu)\mu - \mathbf{D}(\mu)\mu - \mathbf{g}(\eta)$. Note that $\mathbf{M} = \mathbf{M}^* + \Delta\mathbf{M}$, where $\mathbf{M}^*$ and $\Delta\mathbf{M}$ denote the nominal value part and the uncertain value part, respectively.

For a more simplified representation, a lumped disturbance vector ρ, which consists of external disturbances and model parameter uncertainties, is defined by

$$\rho = \mathbf{M}^{-1}\left(\mathbf{U}(\eta,\mu) + \tau_E\right) + \left(\mathbf{M}^{-1} - (\mathbf{M}^*)^{-1}\right)\tau. \tag{5}$$

Therefore, the kinetic model can be written as

$$\dot{\mu} = \rho + (\mathbf{M}^*)^{-1}\tau. \tag{6}$$

This article has been accepted for publication in a future issue of this journal, but has not been fully edited. Content may change prior to final publication. Citation information: DOI 10.1109/TII.2020.3036665, IEEE Transactions on Industrial Informatics

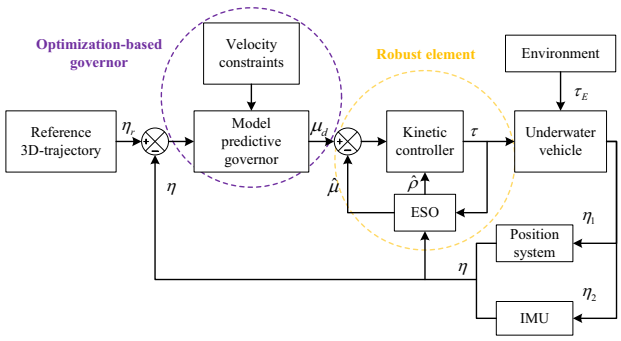

Fig. 1. The proposed control scheme with optimization-based governor and robust element.

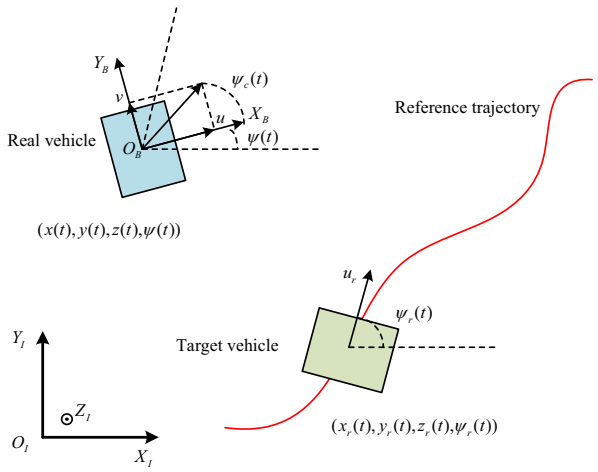

Fig. 2. Description of trajectory tracking in the X-Y view.

B. Control Task and Scheme

The aimed task of this work is to control an underactuated underwater vehicle, which posses actuators to generate surge force, heave force, and yaw torque, to accomplish a 4-DOFs trajectory tracking jointly described by surge motion, swag motion, heave motion, and yaw motion. As illustrated in Fig. 1, the proposed control scheme consists of an optimization-based governor and a robust element.

With respect to the optimization-based governor, a model predictive method is utilized to generate desired velocities with corresponding constrains, which include upper and lower bound, smoothness, and jump range. The desired velocities are formulated by $\mu_d = [u_d, w_d, r_d]^T$, according to which the underactuated underwater vehicle can precisely track the referenced trajectory kinematically.

The crucial part in the robust element is the implementation of ESO. In virtue of the ESO-based robust controller, the lumped disturbance vector can be estimated and compensated to stabilize the controller and improve the capability of disturbance rejection. Especially, if the velocity states are difficult to be obtained in practical applications, by use of the ESO, the observed velocity states can be obtained so that we are able to only utilize position and orientation information to control the underwater vehicle.

III. Model Predictive Governor

A. Tracking Error Model With Underactuated Expression

As shown in Fig. 2, the concept of real vehicle and target vehicle is provided to describe the process of the trajectory tracking. At time t, the kinematic model (1) of the real vehicle can be rewritten in a compact form as

$$\dot{\eta}(t) = g(\eta(t), \mu(t)). \tag{7}$$

Similarly, the target vehicle can be denoted by

$$\dot{\eta}_r(t) = g(\eta_r(t), \mu_r(t)). \tag{8}$$

The kinematic equation (7) is expanded in Taylor series around the reference point $(\eta_r(t), \mu_r(t))$ neglecting the bounded high-order item as follows:

$$\begin{aligned}\dot{\eta}(t) = \dot{\eta}_r(t) + g'(\eta_r(t))(\eta(t) - \eta_r(t)) \\ + g'(\mu_r(t))(\mu(t) - \mu_r(t))\end{aligned} \tag{9}$$

where $g'(\eta_r(t))$ and $g'(\mu_r(t))$ are the jacobian matrices of $g(\eta(t), \mu(t))$ with respect to $\eta(t)$ and $\mu(t)$ at the reference point $(\eta_r(t), \mu_r(t))$, respectively. With this, the kinematic model has the linearization form.

Let $e(t) = \eta(t) - \eta_r(t)$ and $\tilde{\mu} = \mu(t) - \mu_r(t)$. Meanwhile, considering that the dimension related to the uncontrollable velocity state $v(t)$ is excluded from $\tilde{\mu}(t)$, we have the trajectory tracking error model with discrete-time form as follows:

$$e(k+T) = A(k)e(k) + B(k)\tilde{\mu}'(k) \tag{10}$$

where $\tilde{\mu}'(t) = [u(t) - u_r(t), w(t) - w_r(t), r(t) - r_r(t)]^T$,

$$A(k) = \begin{bmatrix} 1 & 0 & 0 & -u_r(t)\sin(\psi_r(t))T \\ 0 & 1 & 0 & u_r(t)\cos(\psi_r(t))T \\ 0 & 0 & 1 & 0 \\ 0 & 0 & 0 & 1 \end{bmatrix}, \tag{11}$$

$$B(k) = TB_e(k) = \begin{bmatrix} \cos(\psi_r(t))T & 0 & 0 \\ \sin(\psi_r(t))T & 0 & 0 \\ 0 & T & 0 \\ 0 & 0 & T \end{bmatrix}. \tag{12}$$

Now that the approximated linear trajectory tracking error model with underactuated form is constructed, by which the practical application has the ability to implement it easily.

B. Heading Angle Compensation

The aforementioned trajectory tracking error model is derived under the assumption that $v(t)$ is set to zero due to the lack of actuator in the sway motion. In reality, the sway velocity cannot identically equal to zero on account of the coupling dynamics. As indicated in Fig. 2, the existence of slideslip angle $\psi_c(t)$ affects the trajectory accuracy and even results in steady state errors. Therefore, it is necessary to introduce a heading angle compensation mechanism for the kinematic trajectory tracking. The heading angle compensation is designed as follows:

$$\psi_r{}'(t) = \psi_r(t) - \psi_c(t) \tag{13}$$

where

$$\psi_c(t) = \arctan\left(\frac{v(t)}{u(t)}\right).$$

This article has been accepted for publication in a future issue of this journal, but has not been fully edited. Content may change prior to final publication. Citation information: DOI 10.1109/TII.2020.3036665, IEEE Transactions on Industrial Informatics

Note that the reference heading angle item in η_r is replaced by ${\psi_r}'$ hereinafter. With the heading angle compensation mechanism, the underactuated underwater vehicle will track the reference trajectory precisely.

C. Cost Function Design for Model Predictive Governor

Commonly, the cost function of this problem can be defined as

$$\begin{aligned} J(k) = &\sum_{i=1}^{N_p} \|(\eta(k+iT|k) - \eta_r(k+iT|k))\|_Q^2 \\ &+ \sum_{i=0}^{N_c-1} \|\Delta\tilde{\mu}'(k+iT|k)\|_R^2 + \varepsilon(k)^T W \varepsilon(k) \end{aligned} \tag{14}$$

where $\eta(k+iT|k)$ and $\eta_r(k+iT|k))$ represent the output state and the reference trajectory state in the predictive horizon, respectively. Meanwhile, $\Delta\tilde{\mu}'(k+iT|k)$ is designated to denote the control increment in the control predictive, where

$$\Delta\tilde{\mu}'(k+iT|k) = \tilde{\mu}'(k+iT|k) - \tilde{\mu}'(k+(i-1)T|k). \tag{15}$$

Note that N_p and N_c are the predicted horizon and the control horizon, respectively, where $N_p \geq 1$ and $N_p \geq N_c \geq 1$ are established. In the last item, $\varepsilon(k) = [\varepsilon_1(k), \varepsilon_2(k), \varepsilon_3(k)]^T$ is the relaxing factor which has the responsibility for preventing from emerging infeasible solutions during execution. With respect to the first item, it describes the tracking capability of the vehicle, where a smaller value means a more precise tracking. Besides, the second item restrains the change of control inputs. Additionally, Q, R, and W are the weighting metrics, where $Q \in R^{4\times4}$ is positive semi-definite, and $R \in R^{3\times3}$ as well as $W \in R^{3\times3}$ are positive definite.

For the simplification of solving (14), a variable is defined as

$$\zeta(k|k) = \begin{bmatrix} e(k|k) \\ \tilde{\mu}'(k-T|k) \end{bmatrix}. \tag{16}$$

In this context, the tracking error model (10) is converted to the following formation

$$\zeta(k+T|k) = \tilde{A}(k)\zeta(k|k) + \tilde{B}(k)\Delta\tilde{\mu}'(k|k) \tag{17}$$

$$e(k|k) = \tilde{C}\zeta(k|k) \tag{18}$$

where $\tilde{A}(k) = \begin{bmatrix} A(k) & B(k) \\ I_{3\times4} & 0_{3\times3} \end{bmatrix}$, $\tilde{B}(k) = [B(k) \quad I_{3\times3}]^T$, and $\tilde{C} = [I_{4\times4} \quad I_{4\times3}]^T$.

We can derive the predicted output expression of the controlled system as follows:

$$\Upsilon(k) = \Gamma(k)\zeta(k|k) + \mathrm{B}(k)\Delta U(k) \tag{19}$$

where the descriptions of $\Upsilon(k)$, $\Gamma(k)$, $\mathrm{B}(k)$, and $\Delta U(k)$ can be obtained in [22].

In this situation, the conventional cost function (14) is converted as below.

$$J(k) = \Upsilon(k)^T\tilde{Q}\Upsilon(k) + \Delta U(k)^T\tilde{R}\Delta U(k) + \varepsilon(k)^T W\varepsilon(k). \tag{20}$$

Then, to solve the optimal problem by QP, it is necessary to reform (20) as

$$\begin{aligned} J(k) = &\frac{1}{2}\begin{bmatrix} \Delta U(k) \\ \varepsilon(k) \end{bmatrix}^T H(k) \begin{bmatrix} \Delta U(k) \\ \varepsilon(k) \end{bmatrix} \\ &+ \Theta(k)\begin{bmatrix} \Delta U(k) \\ \varepsilon(k) \end{bmatrix} + E(k)^T\tilde{Q}E(k) \end{aligned} \tag{21}$$

where

$$H(k) = \begin{bmatrix} 2(\mathrm{B}(k)^T\tilde{Q}\mathrm{B}(k) + \tilde{R}) & 0_{4N_c\times3} \\ 0_{3\times4N_c} & 2W \end{bmatrix},$$
$$\Theta(k) = \begin{bmatrix} 2E(k)^T\tilde{Q}\mathrm{B}(k) & 0 \end{bmatrix}, E(k) = \Gamma(k)\zeta(k|k).$$

Thereinto, $H(k)$ is a Hessian matrix which is utilized to describe a quadratic part of the cost function. Note that $E(k)$, as the tracking error in the predicted horizon, is independent on $\Delta U(k)$ so that omitting it does not affect the cost function.

D. Constraints of the Cost Function

In the kinematic control process, the outputs are expectational control targets for the subsequent kinetic control. Therefore, for a feasible control operation, the velocity constraints are necessary for the control system. With respect to the velocity constraints, there are three primary properties including the lower and upper bound of velocities, the smoothness of control inputs, and the velocity jump range. In this context, the constraints of the cost function can be formulated by the subsequent descriptions.

First, the lower and upper bound of velocities can be denoted by

$$\begin{aligned} \mu'_{\min} \leq \tilde{\mu}'(k+iT|k) \leq \mu'_{\max} - \mu'_r(k), \\ i = 0, 1, 2\cdots N_c - 1. \end{aligned} \tag{22}$$

Second, the smoothness and the velocity jump range are constrained with the following relationship

$$\begin{aligned} \Delta\tilde{\mu}'_{\min} \leq \Delta\tilde{\mu}'(k+iT|k) \leq \Delta\tilde{\mu}'_{\max}, \\ i = 0, 1, 2\cdots N_c - 1. \end{aligned} \tag{23}$$

E. Stability Analysis

Theorem 1: By solving the optimization problem with the cost function (21) subject to (22) and (23), the optimal solution

$$\begin{aligned} [\Delta U^*(k) \quad \varepsilon^*(k)]^T = &[\Delta\tilde{\mu}'^*(k|k) \quad \Delta\tilde{\mu}'^*(k+T|k) \\ &\cdots \quad \Delta\tilde{\mu}'^*(k+(N_c-1)T|k) \\ &\varepsilon_1^*(k) \quad \varepsilon_2^*(k) \quad \varepsilon_3^*(k)]^T \end{aligned} \tag{24}$$

holds. The Lyapunov function $V(k)$ is defined as the optimal cost function $J^*(k)$ at the time instant k. If it is established that $V(k+T) \leq V(k)$ at the time instant $k+T$, then the system (10) is stable.

Proof 1: The lyapunov function $V(k)$ is expressed by

$$\begin{aligned} V(k) &= J^*(k) = \min J(k) \\ &= \min\{\sum_{i=1}^{N_p} \|(\eta(k+iT|k) - \eta_r(k+iT|k))\|_Q^2 \\ &+ \sum_{i=0}^{N_c-1} \|\Delta\tilde{\mu}'(k+iT|k)\|_R^2 + \varepsilon(k)^T W\varepsilon(k)\}. \end{aligned} \tag{25}$$

It is noticeable that $V(k) \geq 0$ always holds for $k \neq 0$. Meanwhile, $V(k) \leq J(k)$ is obtained apparently. To prove $V(k+T) \leq V(k)$, an intermediate variable $J(k+T)$ is considered. The relationship between $J(k+T)$ with $V(k)$ is derived as follows:

$$\begin{aligned}
J(k+T) &= \sum_{i=1}^{N_p} ||(\eta(k+(i+1)T|k+T) \\
&-\eta_r(k+(i+1)T|k+T))||_Q^2 \\
&+ \sum_{i=0}^{N_c-1} \|\Delta\tilde{\mu}'(k+(i+1)T|k+T)\|_R^2 \\
&+ \varepsilon(k+T)^T W \varepsilon(k+T) \\
&= \sum_{i=2}^{N_p} \|(\eta^*(k+iT|k) - \eta_r(k+iT|k))\|_Q^2 \\
&+ \sum_{i=1}^{N_c-1} \left\|\Delta\tilde{\mu}'^*(k+iT|k)\right\|_R^2 + \varepsilon^*(k)^T W \varepsilon^*(k) \\
&= \sum_{i=1}^{N_p} \|(\eta^*(k+iT|k) - \eta_r(k+iT|k))\|_Q^2 \\
&+ \sum_{i=0}^{N_c-1} \left\|\Delta\tilde{\mu}'^*(k+iT|k)\right\|_R^2 + \varepsilon^*(k)^T W \varepsilon^*(k) \\
&- \|(\eta^*(k+T|k) - \eta_r(k+T|k))\|_Q^2 \\
&- \left\|\Delta\tilde{\mu}'^*(k|k)\right\|_R^2 \\
&= V(k) - \|(\eta^*(k+T|k) - \eta_r(k+T|k))\|_Q^2 \\
&- \left\|\Delta\tilde{\mu}'^*(k|k)\right\|_R^2.
\end{aligned} \tag{26}$$

Note that $J(k+T) \leq V(k)$ holds, which leads to that $V(k+T) \leq V(k)$ is satisfied. Therefore, the tracking system (10) is stable. ■

Eventually, referring to [22] the expectational velocity vector produced by the model predictive governor for the kinetic controller can be derived from (10) and (15) as

$$\mu_d = \Delta\tilde{\mu}'^*(k|k) + \tilde{\mu}'(k-T|k) + \mu_r'(k) \tag{27}$$

where $\mu_r'(k) = [u_r(k), w_r(k), r_r(k)]^T$.

IV. ESO-Based Kinetic Control Law

A. Design of ESO

There are two primary assumptions for the dynamics model (4), which are considered in the following ESO design.

Assumption 1 (See in [17]): Due to the velocity-related property of the hydrodynamics item $\mathbf{U}(\eta, \mu)$, the sum of partial derivatives is assumed to be bounded. Namely,

$$||\mathbf{U}(\eta,\mu)|| + ||\partial\mathbf{U}(\eta,\mu)/\partial t|| + ||\partial\mathbf{U}(\eta,\mu)/\partial\mu|| \leq c_1 \tag{28}$$

where c_1 is a positive constant.

Assumption 2 (See in [17]): Considering that the energy limitations of actuators and external forces, the following assumption is reasonable. Namely,

$$||\tau_E|| + ||\dot{\tau}_E|| + ||\tau|| + ||\dot{\tau}|| \leq c_2 \tag{29}$$

where c_2 is a positive constant.

Based on the model of underactuated underwater vehicles (1) and (6), the ESO is designed as

$$\begin{cases} \dot{\hat{\eta}} = -K_1(\hat{\eta} - \eta) + \mathbf{J}(\eta)\hat{\mu} \\ \dot{\hat{\mu}} = -K_2\mathbf{J}(\eta)^T(\hat{\eta} - \eta) + \hat{\rho} + (M^*)^{-1}\tau \\ \dot{\hat{\rho}} = -K_3\mathbf{J}(\eta)^T(\hat{\eta} - \eta) \end{cases} \tag{30}$$

where $\hat{\eta}$, $\hat{\mu}$, and $\hat{\rho}$ are the estimated vectors of η, μ, and ρ, respectively. Besides, $K_1 = diag\{k_{11}, k_{12}, k_{13}, k_{14}\}$, $K_2 = diag\{k_{21}, k_{22}, k_{23}, k_{24}\}$, and $K_3 = diag\{k_{31}, k_{32}, k_{33}, k_{34}\}$ are constant metrics.

By defining $\tilde{\eta}_e = \hat{\eta} - \eta$, $\tilde{\mu}_e = \hat{\mu} - \mu$, and $\tilde{\rho}_e = \hat{\rho} - \rho$ and letting $\tilde{S} = [\tilde{\eta}_e, \tilde{\mu}_e, \tilde{\rho}_e]^T$, it follows that

$$\dot{\tilde{S}} = F_1\tilde{S} - F_2\dot{\rho} \tag{31}$$

where

$$F_1 = \begin{bmatrix} -K_1 & \mathbf{J}(\eta) & 0_{3\times3} \\ -K_2\mathbf{J}(\eta)^T & 0_{3\times3} & I_{3\times3} \\ -K_3\mathbf{J}(\eta)^T & 0_{3\times3} & 0_{3\times3} \end{bmatrix}, F_2 = \begin{bmatrix} 0_{3\times3} \\ 0_{3\times3} \\ I_{3\times3} \end{bmatrix}.$$

Theorem 2: Under the Assumptions 1 and 2, if a positive definite matrix P_r satisfies

$$F_1^T P_r + P_r F_1 + h_p I \leq 0 \tag{32}$$

where h_p is a positive constant, the error dynamics system (31) is input-to-state stable by $\tilde{S}$ being the state vector and $\dot{\rho}$ being the input vector.

Proof 2: Consider a Lyapunov function as

$$V_o = \frac{1}{2}\tilde{S}^T P_r \tilde{S}^T. \tag{33}$$

It is apparent that V_o is positive and bounded as

$$V_o \in \left[\frac{\lambda_{min}(P_r)\left\|\tilde{S}\right\|^2}{2}, \frac{\lambda_{max}(P_r)\left\|\tilde{S}\right\|^2}{2}\right]. \tag{34}$$

Note that, in this paper, $\lambda_{min}(*)$ and $\lambda_{max}(*)$ denote the minimum eigenvalue and maximum eigenvalue of one matrix, respectively.

The time derivative of V is derived with the expression of

$$\dot{V}_o = \frac{1}{2}\tilde{S}^T\left[F_1^T P_r + P_r F_1\right]\tilde{S}^T + \tilde{S}^T P_r F_2(-\dot{\rho}). \tag{35}$$

By substituting (32) into (35), it holds that

$$\dot{V}_o \leq -\frac{h_p}{2}\left\|\tilde{S}\right\|^2 + \left\|\tilde{S}\right\|\|P_r F_2\|\,\|\dot{\rho}\|. \tag{36}$$

When $\left\|\tilde{S}\right\|$ satisfies

$$\left\|\tilde{S}\right\| \geq \frac{2\|P_r F_2\|\,\|\dot{\rho}\|}{h_p\alpha} \tag{37}$$

where $\alpha \in (0,1)$, the time derivative of V_o is bounded by

$$\dot{V}_o \leq -\frac{h_p}{2}(1-\alpha)\left\|\tilde{S}\right\|. \tag{38}$$

This article has been accepted for publication in a future issue of this journal, but has not been fully edited. Content may change prior to final publication. Citation information: DOI 10.1109/TII.2020.3036665, IEEE Transactions on Industrial Informatics

Combining with Assumptions 1 and 2, which endow bound to $\|\dot{\rho}\|$, the system (31) is input-to-state stable with the input vector $\dot{\rho}$. Meanwhile, referring to [18], $\left\|\tilde{S}(t)\right\|$ is bounded as

$$\left\|\tilde{S}(t)\right\| \leq \max\left\{\left\|\tilde{S}(t_0)\right\| e^{-\gamma_s(t-t_0)}, \frac{2\left\|P_r F_2\right\|\|\dot{\rho}\|}{h_p\alpha}\right\} \quad (39)$$

where $\gamma_s = \frac{h_p}{2}(1-\alpha)$. ■

B. Kinetic Control Law

According to the model predictive governor, the expectational velocities are determined. The kinetic control law is designed to follow the reference velocities precisely. From the proposed ESO in (30), the error dynamics of $\hat{u}_e = \hat{u} - u_d$, $\hat{w}_e = \hat{w} - w_d$, and $\hat{r}_e = \hat{r} - r_d$ are expressed as

$$\begin{bmatrix}\dot{\hat{u}}_e\\ \dot{\hat{w}}_e\\ \dot{\hat{r}}_e\end{bmatrix} = \begin{bmatrix}-k_{21}\cos(\psi) & & \\ & -k_{23} & \\ & & -k_{24}\end{bmatrix}\begin{bmatrix}\tilde{x}_e\\ \tilde{z}_e\\ \tilde{\psi}_e\end{bmatrix}^T + \begin{bmatrix}\hat{\rho}_u\\ \hat{\rho}_w\\ \hat{\rho}_r\end{bmatrix} + \begin{bmatrix}m_u^{*-1}\tau_u\\ m_w^{*-1}\tau_w\\ m_r^{*-1}\tau_r\end{bmatrix} - \begin{bmatrix}\dot{u}_d\\ \dot{w}_d\\ \dot{r}_d\end{bmatrix}. \quad (40)$$

To stabilize (40), the control law can be designed as

$$\begin{bmatrix}\tau_u\\ \tau_w\\ \tau_r\end{bmatrix} = \begin{bmatrix}m_u^*(-\kappa_u\hat{u}_e - \hat{\rho}_u)\\ m_w^*(-\kappa_w\hat{w}_e - \hat{\rho}_w)\\ m_r^*(-\kappa_r\hat{r}_e - \hat{\rho}_r)\end{bmatrix} \quad (41)$$

where κ_u, κ_w, and κ_r are positive constants.

By substituting (41) into (40) and defining a dynamics error vector $\mathbf{e}_c = [\hat{u}_e, \hat{w}_e, \hat{r}_e]^T$, we have

$$\dot{\mathbf{e}}_c = -K_\kappa\mathbf{e}_c - K_pL_\eta - d_\mu \quad (42)$$

where $K_\kappa = diag\{\kappa_u, \kappa_w, \kappa_r\}$, $K_p = diag\{k_{21}\cos(\psi), k_{23}, k_{24}\}$, $L_\eta = [\tilde{x}_e, \tilde{z}_e, \tilde{\psi}_e]^T$, and $d_\mu = [\dot{u}_d, \dot{w}_d, \dot{r}_d]^T$.

Theorem 3: The error dynamics system (42) with the state vector $\mathbf{e}_c$ and the input vector d_μ is input-to-state stable.

Proof 3: The Lyapunov function is constructed as

$$V_g = \frac{1}{2}\|\mathbf{e}_c\|^2. \quad (43)$$

The time derivative of V_g is derived as follows:

$$\dot{V}_g = -\mathbf{e}_c^TK_\kappa\mathbf{e}_c - L_\eta^TK_p\mathbf{e}_c - d_\mu^T\mathbf{e}_c. \quad (44)$$

Note that

$$\begin{aligned}\dot{V}_g &\leq -\lambda_{min}(K_\kappa)\|\mathbf{e}_c\|^2 + \lambda_{max}(K_p)\|L_\eta\|\|\mathbf{e}_c\| \\ &\quad + \|d_\mu\|\|\mathbf{e}_c\| \\ &\leq -\lambda_{min}(K_\kappa)\|\mathbf{e}_c\|^2 + \lambda_{max}(K_p)\left\|\tilde{S}\right\|\|\mathbf{e}_c\| \\ &\quad + \|d_\mu\|\|\mathbf{e}_c\|.\end{aligned} \quad (45)$$

When

$$\|\mathbf{e}_c\| \leq \frac{\lambda_{\max}(K_p)\left\|\tilde{S}\right\| + \|d_\mu\|}{\lambda_{\min}(K_\kappa)\alpha_0} \quad (46)$$

with $\alpha_0 \in (0,1)$, it holds that

$$\dot{V}_g \leq -(1-\alpha_0)\lambda_{\min}(K_\kappa)\|\mathbf{e}_c\|^2. \quad (47)$$

TABLE I
CONTROL PARAMETERS

Model predictive governor	
N_p	30
N_c	20
Q	$3I_{4N_p\times 4N_p}$
R	$5I_{3N_c\times 3N_c}$
W	$10I_{3\times 3}$
$\mu'_{\min}$	$[-0.5; -0.54; -0.54]$
$\mu'_{\max}$	$[0.5; 0.54; 0.54]$
$\Delta\tilde{\mu}'_{\max}$	$[0.08; 0.12; 0.12]$
$\Delta\tilde{\mu}'_{\min}$	$[-0.08; -0.12; -0.12]$
ESO-based controller	
$K1$	$diag\{100, 100, 100, 100\}$
$K2$	$diag\{1000, 1000, 1000, 1000\}$
$K3$	$diag\{2000, 2000, 2000, 2000\}$
K_κ	$diag\{1.5, 2.0, 1.3\}$

Associating with (39), the error dynamics system (42) with the state vector $\mathbf{e}_c$ and the input vector d_μ is input-to-state stable, where $\|\mathbf{e}_c(t)\|$ satisfies

$$\|\mathbf{e}_c(t)\| \leq \max\left\{\|\mathbf{e}_c(t_0)\|e^{-\gamma_e(t-t_0)}, \frac{\lambda_{\max}(K_p)\left\|\tilde{S}\right\| + \|d_\mu\|}{\lambda_{\min}(K_\kappa)\alpha_0}\right\} \quad (48)$$

with $\gamma_e = (1-\alpha_0)\lambda_{\min}(K_\kappa)$. ■

V. SIMULATION ANALYSIS AND EXPERIMENTAL RESULTS

A. 3D Trajectory Tracking Performance

To verify the feasibility of the proposed control scheme, briefly named MPCESO below, we conduct some simulation analyses by using the professional sofware. Referring to [3], the model parameters of the simulated underactuated underwater vehicle are $\mathbf{M} = diag\{121.8, 127, 134.1, 33.87\}$, $\mathbf{D}(\mu) = diag\{13+50|u|, 14.3+50.2|v|, 21.2+64.7|w|, 19.2+84.1|r|\}$, $\mathbf{g}(\eta) = 0$, and $\mathbf{C}(\mu)$ can be derived according to $\mathbf{M}$ [30].

The nominal mass metric is set as $\mathbf{M}^* = diag\{100, 100, 100, 25\}$. Meanwhile, the actuated forces in the swag and heave direction are bounded between -20 N and 20 N, and the actuated torque in the yaw direction is bounded between -15 Nm and 15 Nm.

The referenced 3D trajectory with respect to the time t is described by

$$\begin{cases} x_r(t) = 6\sin(0.05\mathrm{t}) \\ y_r(t) = 5 - 6\cos(0.05\mathrm{t}) \\ z_r(t) = 0.01t \end{cases} \quad (49)$$

whose shape is a standard spiral line with radius of 6 m. Additionally, the control parameters selected in the simulation are listed in Table I.

To verify the 3D trajectory tracking performance, the original state vector of the vehicle is set as $[0, -2, 0, 0]^T$ and the external disturbance $\tau_E = \beta\tau_{\sin}$ is introduced to the vehicle by a sinusoidal signal with frequency of 1 rad/s. Note that gains of the sinusoidal signal are related to different values of the positive constant β. Meanwhile, the total simulation time is set to 130 s. With $\beta = 3.0$, the curves of tracking trajectory are shown in Fig. 3. To analyze the tracking error results quantificationally, the root mean square (RMS) error is employed to evaluate tracking accuracy. It is noticeable in

This article has been accepted for publication in a future issue of this journal, but has not been fully edited. Content may change prior to final publication. Citation information: DOI 10.1109/TII.2020.3036665, IEEE Transactions on Industrial Informatics

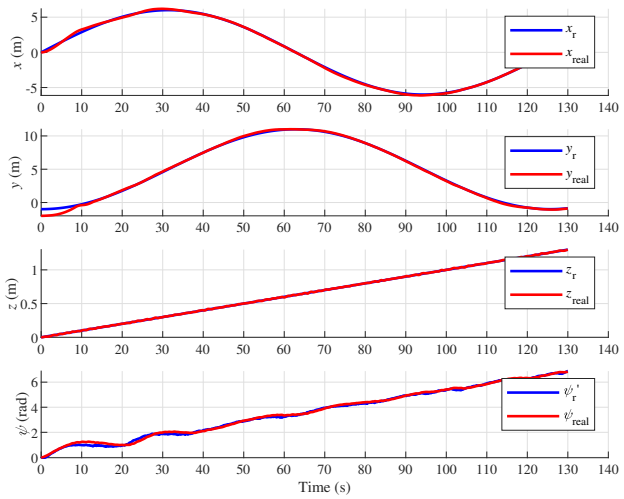

Fig. 3. Tracking trajectory of the underactuated underwater vehicle.

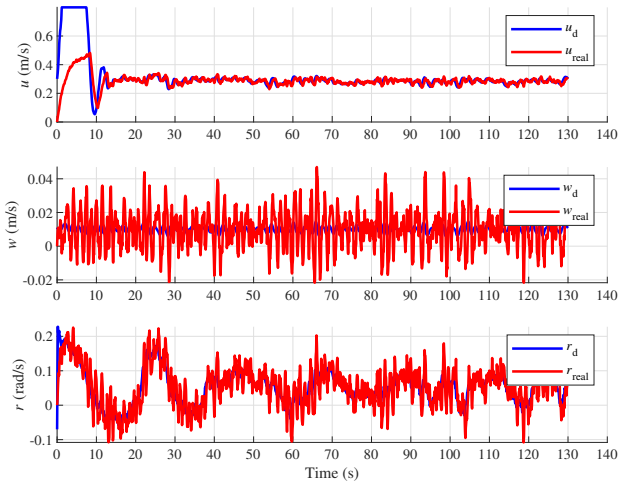

Fig. 4. Coordination between the model predictive governor and the kinetic controller.

Fig. 3 that after 90 s the tracking process reached the steady state. The steady RMS errors in surge, sway, heave, and yaw are 0.074 m, 0.079 m, 0.005 m, and 0.081 rad, respectively. Due to the underactuated property, errors in the horizontal plane are apparently larger than one in the vertical plane. However, the accuracy is satisfactory for the normal operations and voyages.

For a more intuitional perception for the coordination between the model predictive governor and the kinetic controller, the velocity tracking performance is shown in Fig. 4. Note that the blue lines denote the expectational velocities produced by the model predictive governor, which satisfy the constrains of velocity bound, smoothness, and jump ranges, basically. On account of the demand of sharp adjustment at the initial state, the expectational velocities are with fluctuations in the initial stage. However, the aforementioned phenomenon will not destroy the whole tracking process. Besides, the velocity tracking performance is evaluated by the RMS errors, where the RMS velocity tracking errors after 90 s in u, w, and r are 0.021 m/s, 0.012 m/s, and 0.040 rad/s, respectively. The high-enough velocity tracking precision demonstrates the feasibility of the coordination between the model predictive governor and the kinetic controller.

Furthermore, the estimation performance of the ESO is evaluated in Figs. 5 and 6. Thereinto, Fig. 5 shows the capability of lumped disturbance estimation, where the steady estimation RMS errors for ρ_u, ρ_w, and ρ_r are 0.085 m/s^2, 0.055 m/s^2, and 0.211 rad/s^2, respectively. In this context, the accurate observed lumped disturbances will improve the anti-disturbance property of the controller. Besides, the velocity estimation performance is illustrated in Fig. 6. Note that the steady velocity estimation RMS errors in surge, sway, heaven, and yaw are 0.021 m/s, 0.040 m/s, 0.008 m/s, and 0.055 rad/s, respectively, where the simulation results indicate that the MPCESO is sufficient to accomplish the trajectory tracking control just in virtue of the position and orientation information. Besides, the control input graph is shown in Fig. 7, where the sinusoidal shapes of forces and torque demonstrate the anti-interference capability of the controller

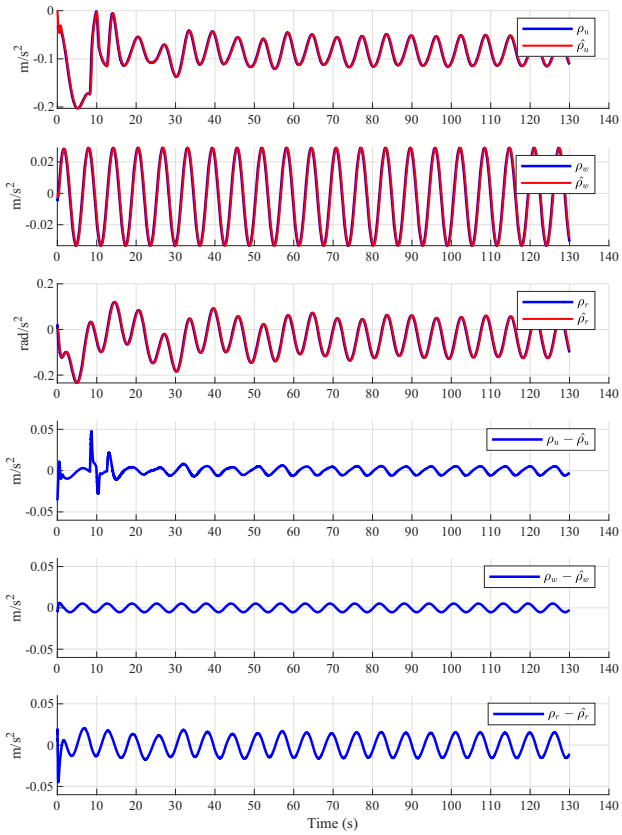

Fig. 5. Observation results of lumped disturbances.

against the sinusoidal external disturbances introduced to the underwater vehicle.

Additionally, the robustness of the 3D trajectory tracking controller is tested under the different conditions of the lumped disturbances. With values of β varying in $\{3.0, 5.0, 8.0\}$, the rejecting disturbance simulations are conducted. The steady RMS tracking errors under different conditions of lumped disturbances are computed in Table II. It is noticeable that the tracking quality is insensible to the enhanced lumped disturbance. The simulation results demonstrate the robustness

This article has been accepted for publication in a future issue of this journal, but has not been fully edited. Content may change prior to final publication. Citation information: DOI 10.1109/TII.2020.3036665, IEEE Transactions on Industrial Informatics

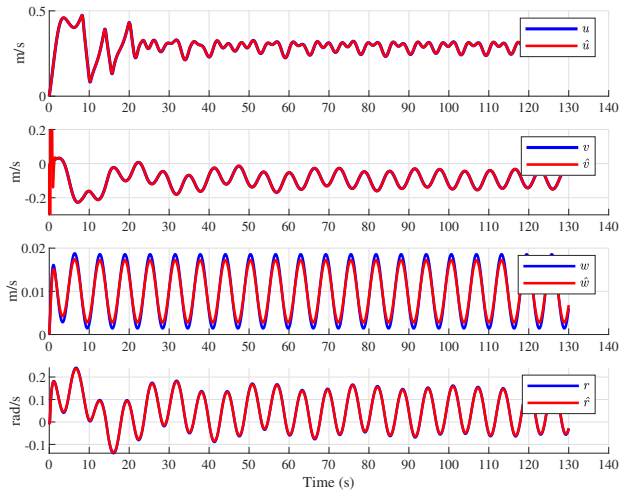

Fig. 6. Estimation results of velocities.

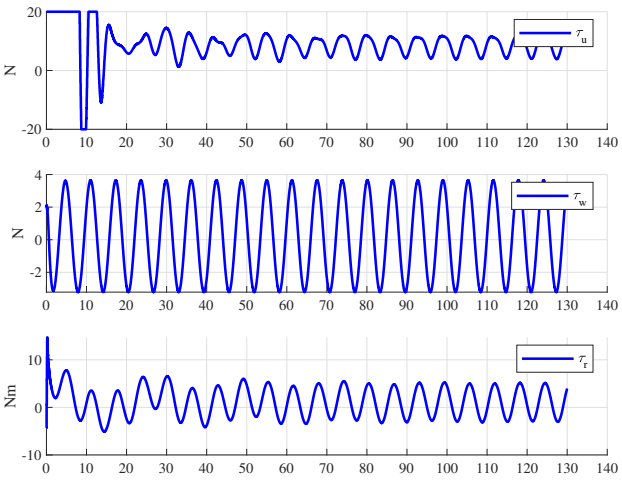

Fig. 7. Control input graph.

TABLE II
STEADY RMS TRACKING ERRORS WITH DIFFERENT DISTURBANCES

	$\beta = 3.0$	$\beta = 5.0$	$\beta = 8.0$
Surge RMS e_x (m)	0.074	0.074	0.085
Sway RMS e_y (m)	0.079	0.082	0.090
Heave RMS e_z (m)	0.005	0.008	0.009
Yaw RMS e_ψ (rad)	0.081	0.085	0.093

of the proposed control scheme. Furthermore, to investigate the effect of disturbance on the convergence bound, a fitting curve describing the relationship between disturbance intensity and the RMS error of the surge tracking is plotted in Fig. 8. It is apparent that when $\beta \geq 12$ holds, the convergence of the tracking control will get worse rapidly. One primary reason for the convergence destruction is that the control input bounds will constraint the resisting disturbance capability of the underwater vehicle even though the disturbances could be estimated accurately.

B. Comparative Simulations

To reveal the superiorities of the proposed control scheme, there are two simulations about comparison conducted in this paper. The first comparison is to validate the efficiency of the heading angle compensation mechanism. Under the disturbances with $\beta = 3.0$, the steady RMS tracking errors of MPCESO with the compensation mechanism and one without the compensation mechanism are listed in Table III. It is concluded that notably larger steady tracking errors in surge and sway exist in the situation without the compensation mechanism.

In the second comparative simulation, the MPCESO is compared with the computed-torque-like control method in [12] and the conventional PID controller, respectively. With $\beta = 8.0$, the steady RMS errors of the three methods are calculated in Table IV. From the above, the steady RMS errors of MPCESO are distinctly smaller than ones of the others, which demonstrates the superior 3D trajectory tracking performances of MPCESO.

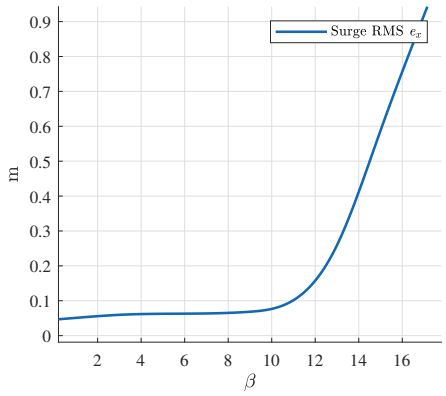

Fig. 8. The relationship between disturbance intensities and RMS errors.

TABLE III
COMPARISON OF COMPREHENSION MECHANISMS

	With compensation	Without compensation
Surge RMS e_x (m)	0.074	0.602
Sway RMS e_y (m)	0.079	0.681
Heave RMS e_z (m)	0.005	0.004
Yaw RMS e_ψ (rad)	0.081	0.340

TABLE IV
TRACKING ERRORS OF DIFFERENT METHODS

	MPCESO	Method in [12]	PID
Surge RMS e_x (m)	0.089	0.132	0.189
Sway RMS e_y (m)	0.091	0.200	0.282
Heave RMS e_z (m)	0.009	0.014	0.026
Yaw RMS e_ψ (rad)	0.094	0.177	0.185

C. Additional Robust Test for MPCESO

In the aforementioned simulations, the 4-DOF underwater vehicle model is utilized to evaluate the feasibility of MPCESO under the reasonable assumption of none roll and pitch angles. However, it is necessary to conduct a more near-realistic robust test with a 6-DOF underwater vehicle model influenced by the discontinued marine currents.

With respect to the 6-DOF model, the roll and pitch movements are considered and the center of body-fixed frame does not coincide the center of gravity. In this situation, the model

This article has been accepted for publication in a future issue of this journal, but has not been fully edited. Content may change prior to final publication. Citation information: DOI 10.1109/TII.2020.3036665, IEEE Transactions on Industrial Informatics

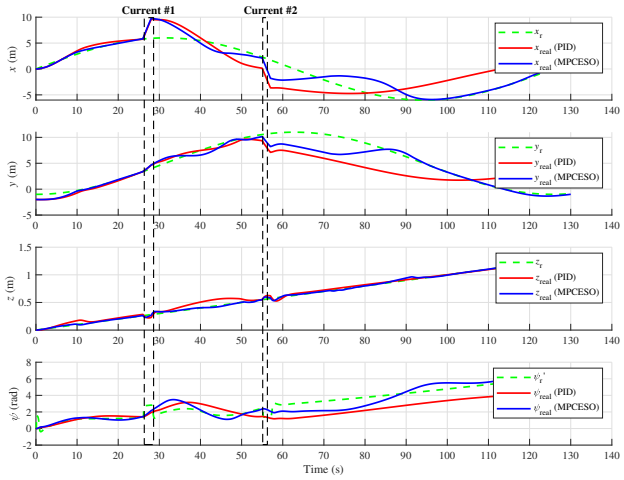

Fig. 9. Tracking trajectory of the 6-DOF underwater vehicle faced with marine current influence.

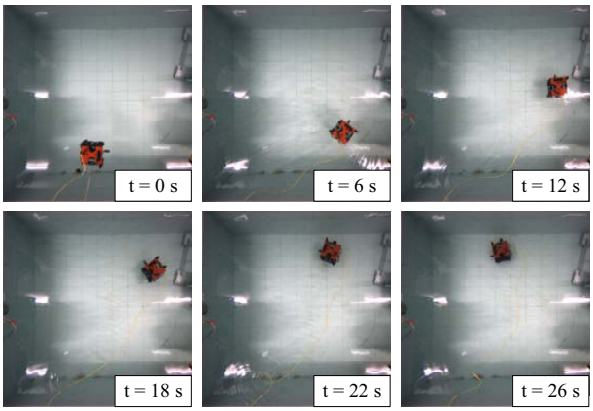

Fig. 10. Video snapshots of the trajectory tracking experiment.

parameters of the simulated underactuated underwater vehicle are $\mathbf{M} = diag\{121.8, 127, 134.1, 33.87, 33.87, 33.62\}$, $\mathbf{D}(\mu) = diag\{13 + 50|u|, 14.3 + 50.2|v|, 21.2 + 64.7|w|, 18 + 73.8|p|, 24.3 + 101.7|q|, 19.2 + 84.1|r|\}$, and $\mathbf{g}(\eta) \neq 0$. Meanwhile, two-time marine current impacts with different directions and strengthens occur at the simulation time interval from 26 s to 28 s and the time interval from 56 s to 57 s, respectively. The marine current is denoted by a velocity vector referring to the inertial frame, which will add incremental values to the velocities of underwater vehicle eventually disturbing the tracking movement. The simulation result of additional robust test for the trajectory tracking is illustrated in Fig. 9. Note that **Current #1** and **Current #2** are denoted by $[1.9, 0.3, -0.1, 0.0, 0.0, 0.15]^T$ and $[-1.8, -1.15, 0.1, 0.05, 0.005, -0.1]^T$, respectively. It can be concluded that the trajectory tracking controller designed from the 4-DOF model is robust enough for a 6-DOF underwater vehicle model even in the situation with sudden turbulence flow effects. Moreover, it is apparent that the disturbance rejection performance of MPCESO is better than the classical PID controller.

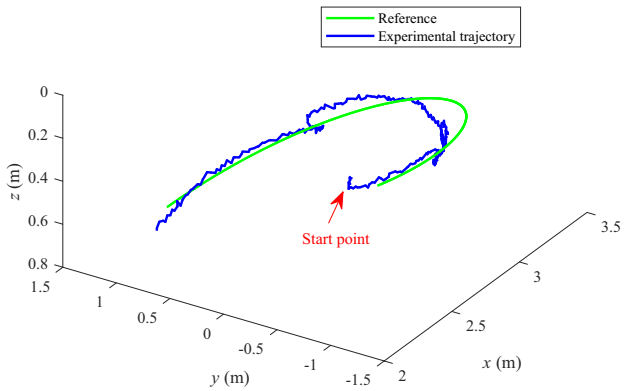

Fig. 11. Tracking trajectory of the real underwater vehicle.

D. Experimental Verification in Lab Environment

To verify the performance of the proposed controller, an experiment with an underactuated 4-DOF underwater vehicle has been conducted in a laboratory environment. Note that positions in the horizontal plane are obtained by the global camera, the depth data are collected from a pressure sensor, and the yaw angle is measured by the IMU algorithm. The referenced trajectory is described as follows:

$$\begin{cases} x_r(t) = 2 + 1.4\sin(0.011\mathrm{t}) \\ y_r(t) = 1.4\cos(0.011\mathrm{t}) \\ z_r(t) = 0.02t \end{cases} \tag{50}$$

The starting position and orientation of the underwater vehicle was set as $(2.02\ \mathrm{m}, -1.15\ \mathrm{m}, 0.00\ \mathrm{m}, -0.11\ \mathrm{rad})$, and trajectory tracking performance is illustrated in Figs. 10 and 11. According to the two figures, the feasibility of the proposed method can be demonstrated intuitively. For a quantitative analysis, the steady RMS errors in surge, sway, heave, and yaw are 0.0648 m, 0.0965 m, 0.0267 m, and 0.0724 rad, respectively. According to the system errors from sensors, the tracking accuracy is satisfactory.

E. Discussion

According to the aforementioned comprehensive simulation analysis and experimental verification, the proposed MPCESO scheme is demonstrated to be a feasible and robust trajectory tracking control method. Thereinto, the robust test, the convergence investigation, and the comparison simulation with other methods in the literature indicate that the proposed control scheme benefitted by the ESO has a satisfactory capability of resisting disturbances ensuring an accurate trajectory tracking performance. The experimental verification implies the guiding significance for the future application prospect in the marine exploration.

In addition to this, there are two notable remarks for the proposed control scheme.

1) The results of simulation and experiment indicate that the controller designed from a relatively simplified 4-DOF model is appropriate for a more complicated 6-DOF model. One primary reason is that the lumped

disturbance vector includes external disturbances, model parameter uncertainties, effects from the relative motion of the water, and effects caused by the dynamics coupling. In this situation, an accurate estimation of the lumped disturbance vector can stabilize the underwater vehicle.

2) With respect to the proposed ESO, the unmeasurable variables are velocities of the underwater vehicle and the measurable variables are positions and orientations. In reality, velocities of the underwater vehicle can be measured using DVL. However, constrained by the loading ability, the underwater vehicle might carry few sensors and electronic instruments. In such a situation, the proposed ESO provides an alternative method at the moment when DVL is out of use.

It goes without saying that a further and intensive study about the disturbances caused by the relative motion of the water and accumulated errors of sensors should be conducted so as to improve the control performance of the underwater vehicle.

VI. Conclusion and Future Work

Considering the underactuated property, velocity constraint, and lumped disturbance in the 3D trajectory tracking task, a control scheme consisting of model predictive governor and ESO-based controller is implemented in this paper. The model predictive governor employs the underactuated tracking error model and heading angle compensation mechanism to accomplish a precise kinematic tracking. Besides, the ESO-based controller is utilized to reject lumped disturbances and control the vehicle just by use of the position and orientation information. Theoretical analysis, simulation results, and laboratorial experiment verify the feasibility of the proposed control scheme.

In the future, the control scheme will be implemented on the underactuated underwater vehicles applied to field aquatic environmental monitoring so as to verify the robustness of the controller in the more complicated environments.

References

[1] K. Alam, T. Ray, and S. G. Anavatti, "Design optimization of an unmanned underwater vehicle using low- and high-fidelity models," *IEEE Trans. Syst., Man, Cybern., Syst.*, vol. 47, no. 11, pp. 2794–2808, Nov. 2017.

[2] I. Jawhar, N. Mohamed, J. Al-Jaroodi, and S. Zhang, "An architecture for using autonomous underwater vehicles in wireless sensor networks for underwater pipeline monitoring," *IEEE Trans. Ind. Inform.*, vol. 15, no. 3, pp. 1329–1340, Mar. 2019.

[3] R. Cui, C. Yang, Y. Li, and S. Sharma, "Adaptive neural network control of AUVs with control input nonlinearities using reinforcement learning," *IEEE Trans. Syst., Man, Cybern., Syst.*, vol. 47, no. 6, pp. 1019–1029, Jun. 2017.

[4] R. Wang, S. Wang, Y. Wang, M. Tan, and J. Yu, "A paradigm for path following control of a ribbon-fin propelled biomimetic underwater vehicle," *IEEE Trans. Syst., Man, Cybern., Syst.*, vol. 49, no. 3, pp. 482–493, Mar. 2019.

[5] L. Qiao and W. Zhang, "Trajectory tracking control of AUVs via adaptive fast nonsingular integral terminal sliding mode control," *IEEE Trans. Ind. Inform.*, vol. 16, no. 2, pp. 1248–1258, Feb. 2020.

[6] Y. Chen, R. Zhang, X. Zhao, and J. Gao, "Adaptive fuzzy inverse trajectory tracking control of underactuated underwater vehicle with uncertainties," *Ocean Eng.*, vol. 121, pp. 123–133, May 2016.

[7] C. D. Makavita, S. G. Jayasinghe, H. D. Nguyen, and D. Ranmuthugala, "Experimental study of command governor adaptive control for unmanned underwater vehicles," *IEEE Trans. Control Syst. Technol.*, vol. 27, no. 1, pp. 332–345, Jan. 2019.

[8] C. P. Bechlioulis, G. C. Karras, S. Heshmati-Alamdari, and K. J. Kyriakopoulos, "Trajectory tracking with prescribed performance for underactuated underwater vehicles under model uncertainties and external disturbances," *IEEE Trans. Control Syst. Technol.*, vol. 25, no. 2, pp. 429–440, Mar. 2017.

[9] W. He, Z. Yin, and C. Sun, "Adaptive neural network control of a marine vessel with constraints using the asymmetric barrier lyapunov function," *IEEE Trans. Cybern.*, vol. 47, no. 7, pp. 1641–1651, Jul. 2017.

[10] H. Li, P. Xie, and W. Yan, "Receding horizon formation tracking control of constrained underactuated autonomous underwater vehicles," *IEEE Trans. Ind. Electron.*, vol. 64, no. 6, pp. 5004–5013, Jul. 2017.

[11] R. Cui, L. Chen, C. Yang, and M. Chen, "Extended state observer-based integral sliding mode control for an underwater robot with unknown disturbances and uncertain nonlinearities," *IEEE Trans. Ind. Electron.*, vol. 64, no. 8, pp. 6785–6795, Aug. 2017.

[12] A. Wadi, S. Mukhopadhyay, and J. Lee, "A novel disturbance-robust adaptive trajectory tracking controller for a class of underactuated autonomous underwater vehicles," *Ocean Eng.*, vol. 189, Art. no. 106377, 2019.

[13] M. H. Khodayari and S. Balochian, "Modeling and control of autonomous underwater vehicle (AUV) in heading and depth attitude via self-adaptive fuzzy PID controller," *J. Mar. Sci. Technol.*, vol. 20, pp. 559–578, Mar. 2015.

[14] S. P. Bong, "Neural network-based tracking control of underactuated autonomous underwater vehicles with model uncertainties," *J. Dyn. Sys., Meas., Control*, vol. 137, no. 2, pp. 1–7, Sep. 2014.

[15] C. Yu, X. Xiang, Q. Zhang, and G. Xu, "Adaptive fuzzy trajectory tracking control of an underactuated autonomous underwater vehicle subject to actuator saturation," *Int. J. Fuzzy Syst.*, vol. 10, pp. 269–279, Oct. 2017.

[16] T. Elmokadema, M. Zribia, and K. Youcef-Toumib, "Terminal sliding mode control for the trajectory tracking of underactuated Autonomous Underwater Vehicles," *Ocean Eng.*, vol. 129, pp. 613–625, Jan. 2017.

[17] Z. Peng and J. Wang, "Output-feedback path-following control of autonomous underwater vehicles based on an extended state observer and projection neural networks," *IEEE Trans. Syst., Man, Cybern., Syst.*, vol. 48, no. 4, pp. 535–544, Apr. 2018.

[18] Z. Peng, J. Wang, and Q. Han, "Path-following control of autonomous underwater vehicles subject to velocity and input constraints via neurodynamic optimization," *IEEE Trans. Ind. Electron.*, vol. 66, no. 11, pp. 8724–8732, Nov. 2019.

[19] Z. Peng, J. Wang, and J. Wang, "Constrained control of autonomous underwater vehicles vased on command optimization and disturbance estimation," *IEEE Trans. Ind. Electron.*, vol. 66, no. 5, pp. 3627–3635, May 2019.

[20] Y. Yuan, F. Sun, and H. Liu, "Resilient control of cyber-physical systems against intelligent attacker: a hierarchal Stackelberg game approach," *Int. J. Syst. Sci.*, vol. 47, pp. 2067–2077, Jan. 2016.

[21] Y. Song, X. Huang, and C. Wen, "Tracking control for a class of unknown nonsquare MIMO nonaffine systems: A deep-rooted information based robust adaptive approach," *IEEE Trans. Autom. Control*, vol. 61, no. 10, pp. 3227–3233, Oct. 2016.

[22] H. Yang, M. Guo, Y. Xia, and L. Cheng, "Trajectory tracking for wheeled mobile robots via model predictive control with softening constraints," *IET Control Theory Appl.*, vol. 12, no. 2, pp. 206–214, Jan. 2018.

[23] J. Wang, Z. Wu, M. Tan, and J. Yu, "Model predictive control-based depth control in gliding motion of a gliding robotic dolphin," *IEEE Trans. Syst., Man, Cybern., Syst.*, 2019, to be published, doi: 10.1109/TSMC.2019.2956531.

[24] B. N. Rath and B. Subudhi, "Extreme learning-based non-linear model predictive controller for an autonomous underwater vehicle: simulation and experimental results," *IET Cyber Syst. Robot.*, vol. 1, no. 2, pp. 45–54, Oct. 2019.

[25] C. Shen, Y. Shi, and B. Buckham, "Trajectory tracking control of an autonomous underwater vehicle using Lyapunov-based model predictive control," *IEEE Trans. Ind. Electron.*, vol. 65, no. 7, pp. 5796–5805, Dec. 2017.

[26] S. Heshmati-Alamdari, G. C. Karras, P. Marantos, and K. J. Kyriakopoulos, "A robust predictive control approach for underwater robotic vehicles," *IEEE Trans. Control Syst. Technol.*, vol. 28, no. 6, pp. 2352–2363, Nov. 2020.

[27] J. Na, X. Ren, and D. Zheng, "Adaptive control for nonlinear purefeedback systems with high-order sliding mode observer," *IEEE Trans. Neural Netw. Learn. Syst.*, vol. 24, no. 3, pp. 370–382, Jan. 2013.
[28] D. Fernandes, A. J. Sorensen, K. Y. Pettersen, and D. C. Donha, "Output feedback motion control system for observation class ROVs based on a high-gain state observer: Theoretical and experimental results," *Control Eng. Practice*, vol. 39, pp. 90–102, Jun. 2015.
[29] J. Yao, Z. Jiao, and D. Ma, "Extended-state-observer-based output feedback nonlinear robust control of hydraulic systems with backstepping," *IEEE Trans. Ind. Electron.*, vol. 61, no. 11, pp. 6285–6293, Feb. 2014.
[30] T. Fossen, "Guidance and control of ocean vehicles," NewYork, NY, USA: Wiley, 1994.

Shihan Kong received the B.E. degree in automation from the School of Control Science and Engineering, Shandong University, Jinan, China, in 2016. He is currently pursuing the Ph.D. degree in control theory and control engineering from the Institute of Automation, Chinese Academy of Sciences, Beijing, China.

His current research interests include intelligent control, underwater robotics, and underwater robot vision.

Jinlin Sun received the B.E. degree in automation from Jiangsu University, Zhenjiang, China, in 2016. He is currently pursuing the Ph.D. degree in control theory and control engineering with the Institute of Automation, Chinese Academy of Sciences, Beijing, China.

He visited the University of Rhode Island, Kingston, RI, USA, from 2019 to 2020. His current research interests include disturbance estimation, adaptive control, and their applications.

Changlin Qiu received the B.E. degree in automation from the School of Control Science and Engineering, Shandong University, Jinan, China, in 2019. He is currently pursuing the Ph.D. degree in control theory and control engineering from the Institute of Automation, Chinese Academy of Sciences, Beijing, China.

His current research interests include underwater robotics and underwater robot vision.

Zhengxing Wu received the B.E. degree in logistics engineering from the School of Control Science and Engineering, Shandong University, Jinan, China, in 2008 and the Ph.D. degree in control theory and control engineering from the Institute of Automation, Chinese Academy of Sciences (IACAS), Beijing, China, in 2015.

He is currently an Associate Professor with the State Key Laboratory of Management and Control for Complex Systems, IACAS. His current research interests include fast maneuvers of bio-inspired robotic fish and gliding motions of robotic dolphins.

Junzhi Yu (SM'14) received the B.E. degree in safety engineering and the M.E. degree in precision instruments and mechanology from the North University of China, Taiyuan, China, in 1998 and 2001, respectively, and the Ph.D. degree in control theory and control engineering from the Institute of Automation, Chinese Academy of Sciences, Beijing, China, in 2003.

From 2004 to 2006, he was a Post-Doctoral Research Fellow with the Center for Systems and Control, Peking University, Beijing. He was an Associate Professor with the Institute of Automation, Chinese Academy of Sciences in 2006, where he was a Full Professor in 2012. In 2018, he joined the College of Engineering, Peking University as a Tenured Full Professor. His current research interests include intelligent robots, motion control, and intelligent mechatronic systems.